Advances in Concrete Construction, *Vol. 15, No. 1 (2023) 23-39*
https://doi.org/10.12989/acc.2023.15.1.023

Effect of length and content of steel fibers on the flexural and impact performance of self-compacting cementitious composite panels

Denise-Penelope N. Kontoni*[1,2], Behnaz Jahangiri [3a], Ahmad Dalvand [3,4b] and Mozafar Shokri-Rad [3c]

[1] *Department of Civil Engineering, School of Engineering, University of the Peloponnese, GR-26334 Patras, Greece*
[2] *School of Science and Technology, Hellenic Open University, GR-26335 Patras, Greece*
[3] *Faculty of Engineering, Lorestan University, Khorramabad, Iran*
[4] *Centre for Infrastructure Engineering, Western Sydney University, Penrith NSW 2751, Australia*

(*Received March 28, 2021, Revised December 13, 2022, Accepted January 19, 2023*)

Abstract. One of the important problems of concrete placing is the concrete compaction, which can affect the strength, durability and apparent quality of the hardened concrete. Therefore, vibrating operations might be accompanied by much noise and the need for training the involved workers, while inappropriate functioning can result in many problems. One of the most important methods to solve these problems is to utilize self-compacting cementitious composites instead of the normal concrete. Due to their benefits of these new materials, such as high tensile, compressive, and flexural strength, have drawn the researchers' attention to this type of cementitious composite more than ever. In this experimental investigation, six mixing designs were selected as a base to acquire the best mechanical properties. Moreover, forty-eight rectangular composite panels with dimensions of 300 mm × 400 mm and two thickness values of 30 mm and 50 mm were cast and tested to compare the flexural and impact energy absorption. Steel fibers with volume fractions of 0%, 0.5% and 1% and with lengths of 25 mm and 50 mm were imposed in order to prepare the required cement composites. In this research, the composite panels with two thicknesses of 30 mm and 50 mm, classified into 12 different groups, were cast and tested under three-point flexural bending and repeated drop weight impact test, respectively. Also, the examination and comparison of flexural energy absorption with impact energy absorption were one of the other aims of this research. The obtained results showed that the addition of fibers of longer length improved the mechanical properties of specimens. On the other hand, the findings of the flexural and impact test on the self-compacting composite panels indicated a stronger influence of the long-length fibers.

Keywords: cementitious composites; flexural strength; impact strength; self-compacting; steel fibers; tensile strength

1. Introduction

In recent years, fiber-reinforced cementitious composites have observed significant advancements (Afzali-Naniz and Mazloom 2019). Most of these advancements lay on the further development of the mortar, various types of fibers, fiber-mortar interactions, and the production process of the applied composites (Banthia and Sappakittipakorn 2007, Wild *et al*. 1995). One other issue can be the introduction of a new generation of plasticizers (superplasticizers) with the possibility of achieving high strength with a minimal decrease in mortar performance. Moreover, adding materials, such as silica fume and fly ash, and a better understanding of how they affect the porosity, resistivity, and durability of mortar have also improved the behavior of these materials (Wild *et al*. 1995, Ozawa *et al*. 1996).

Moreover, using self-compacting concrete as a high-performance material is rapidly utilized by some researchers in experimental investigations (Benyamina *et al*. 2019, Djelloul *et al*. 2018, Lenka and Panda 2017, Sahraoui and Bouziani 2019, Salhi *et al*. 2017, Senthil *et al*. 2016). All these issues have caused fundamental progress in the preparation and modeling of composites' behaviors. Currently, concrete materials are widely used in engineering structures. These materials, compared to other materials, have more weight in the cost unit. Concrete has high resistance against fire and has high-energy absorption. One of the major weaknesses can be its higher vulnerability to damage under intensive dynamic loads, which is due to the lack of high tensile force tolerations (Okamura and Ouchi 1998); therefore, the impact behavior of concrete material is different from its other mechanical properties (Karanth *et al*. 2017, Kim *et al*. 2019). Also, some investigations were fulfilled on the impact behavior of beam and slab members (Ahmadi *et al*. 2020, Şengel *et al*. 2022, Zheng *et al*. 2022). The addition of a new type of fibers, including recycled waste materials, has been considered by some researchers to examine the impact behavior of concrete specimens under impact loading (Dalvand and Ahmadi 2021, Huang *et al*. 2021, Liu *et al*. 2022). Besides, adding new fiber can be improved the mechanical and impact characteristics of concrete, especially in self-compacting cementitious

*Corresponding author, Associate Professor,
E-mail: kontoni@uop.gr
[a] M.Sc. Graduate,
E-mail: behnaz.jahangiri1988@gmail.com
[b] Associate Professor, E-mail: dalvand.a@lu.ac.ir
[c] Assistant Professor, E-mail: shokrirad.m@lu.ac.ir

ISSN: 2287-5301 (Print), 2287-531X (Online)

concrete material, due to their ability to increase the integrity of the matrix. Furthermore, the crack propagation mode is important for the impact behavior of concrete materials and engineered cementitious composites (ECC); thus, some researchers have considered the crack behavior of new ECC materials by modeling crack characteristics (Huang *et al*. 2021). By using fibers in concrete, the rate of crack development reduces and results in the ductility of concrete. Some examples of these fibers are steel, carbon, glass, and polymer fibers. Fibrous concrete has good properties such as ductility, high-energy absorption, and stability against cracking, which have accordingly raised many issues at the time of applying them (Okamura and Ozawa 1994, Zhu *et al*. 2001, Mastali *et al*. 2017). In the 1960s, Romualdi and Mandel investigated the effect of steel fibers on the reduction of concrete brittleness (Romualdi and Mandel 1964). This trend continued with the application of other fibers, and in recent years, the combination of various fibers with different lengths has been put on the agenda. The development of knowledge regarding how fibers can affect mortar has led to the compilation of recommendations regarding structural design by the RILEM Institute (Vandewalle *et al*. 2003). Engineered cementitious composites (ECC) have been developed at the University of Michigan, and their tensile ductility has improved considerably due to the regular formation and development of multiple cracks. Also, self-compacting concrete (SCC), a flowable concrete, has the ability to compact due to its own weight (Vivek and Dhinakaran 2017). In these cementitious composites, the content of fibers was reduced to less than 2%. Based on the research carried out from 1993 to 2003, the tensile strength of 4-6 MPa and the tensile ductility of 3-5% were observed for these composites (Li 1993, Li and Yang 2007). Engineered cementitious composites (ECC) can have extensive applications. The application of self-compacting cementitious composites in large-scale construction projects and dense reinforcements is one of the usages of these composites (Kong *et al*. 2003, Karihaloo and Wang 1997). There is also one type of engineered cementitious composites, which can be used in light structures with a low specific weight. Another type of environmentally friendly-engineered cementitious composites has also been constructed (Karihaloo and Wang 1997). Moreover, other types of engineered cementitious composites are being developed that have self-rehabilitation properties (Lepech *et al*. 2008). In other words, such composites are used in order to recover the mechanical properties of materials after suffering damage (Li and Yang 2007, Facconi *et al*. 2016, Muttashar *et al*. 2018, Xu *et al*. 2019a). Concrete is a widely used substance on the earth and is the most consumed construction material worldwide. The use of this material is because of its unique properties, such as high durability and compressive strength. Although the application of traditional vibrated concretes is very popular, the use of ordinary concrete might confront with a number of problems, such as placing it in places with dense reinforcement, complicated molds, and a lack of skilled workers for the concrete vibration. By the vibrating operation, concrete is pushed locally, and this might lead to the release of unintentional bubbles of air after concrete placement. The existence of these bubbles increases the permeability and incurs a risk to concrete durability. Air voids might also reduce the amount of contact between concrete and bars, and this can result in reducing bonding between bars and steel fibers and the expected strength (Xu *et al*. 2019b). This issue is more important for parts such as shear walls and columns in which there are high amounts of dense reinforcement and small concrete sections (Naaman and Reinhardt 2003, Chan *et al*. 2018, Aslani and Nejadi 2012). Although the use of self-compact cementitious composites can deal with a portion of these deficiencies, the use of fibers with the same lengths in self-compact cementitious composites can lead to an unsuitable distribution of fibers in composites (Karimipour *et al*. 2020, Valizadeh *et al*. 2020). Therefore, the application of steel fibers with various lengths in order to increase the uniform distribution of the fibers can be used as a useful method for the dispersion of the fibers in the concrete. Although many researchers have examined concrete panels, there is a scarcity of research on the flexural and impact behavior of these types of self-compacting cementitious composites with different lengths. In the current research, one of the main objectives was a comparison between the flexural energy absorption and impact energy absorption at the composite panels. Also, the length's effect of steel fibers on the specimen's energy absorption was examined in this research. Due to the lack of information in this area, the combination of the flexural, impact, and fiber's length effects was selected as the main variable in this paper. Moreover, some of the self-compacting cementitious base compositions were considered to utilize in this research according to previous experimental works.

2. Experimental program

2.1 Materials

In this research, fine aggregates rock materials were applied after passing through seize No. 8. In addition, in the present investigation, Portland type II cement (produced by Doroud Cement Plant) was used. The specifications of Portland type II cement are presented in Table 1. Also, the maximum aggregate size used in this research was 2.36 mm. Moreover, the water used in this experiment was fresh water, 90% of which was mixed with sand, fly ash, and cement, and the remaining was combined with a superplasticizer solution. A commercial polycarboxylate superplasticizer, namely Dezobuild D. 10, was used. In this experiment, double-ended hook steel fibers with lengths of 25 mm and 50 mm and a diameter of 0.8 mm were used. At first, the sand, fly ash, and cement, were combined together in the mixer for 2-3 min, and then 90% of the water was added to the compositions. Finally, the remaining 10% of water, combined with superplasticizer solution, was added to the compositions. In the last stage, fibers were added to the mixture, and attempts were made to maintain a uniform distribution of fibers. Steel fibers specifications applied in this study are presented in Table 2. In addition, fiber

Table 1 Chemical composition and physical properties of Portland cement and fly ash

Composition	Cement (%)	Fly ash (%)
SiO_2	21.1	72.10
Al_2O_3	4.37	24.70
Fe_2O_3	3.88	1.20
MgO	1.56	0.18
K_2O	0.52	0.50
Na_2O	0.39	0.10
CaO	63.33	0.10
C_3S	51	-
C_2S	22.7	-
C3A	5.1	-
C_4AF	11.9	-
Physical properties		
Specific gravity	3.1	2.30
Specific surface (Cm^2/gr)	3000	3430

Table 2 Mechanical properties of steel fibers

Length (mm)	Diameter (mm)	L/D	Yielding stress (MPa)	Elastic modulus (GPa)	Density (Kg/m^3)
25	0.8	31.25	110	200	7850
50	0.8	62.5	110	200	7850

profiles are shown in Fig. 1. Moreover, all mix designs had the same water-to-cement ratio and aggregate content.

As can be seen from Table 3, six mix designs were utilized to build composite specimens. In this study, the proportions of mixes were proposed based on the previous experience of the authors. The fiber volume fraction percentage for all mix designs was 1%. One mix design was used as a reference mix and did not have any fiber, while three mixing designs had one type of steel fibers, and two mixing designs had composite fiber with different lengths. After casting, the specimens were hardened for 24 h under laboratory conditions to prevent loss of moisture from the specimens. Then, the hardened specimens were demoulded and placed in water until the time of the tests.

2.2 Composite panel preparation

To investigate the impact resistance and flexural performance of mixing designs, 48 composite panels have been made and tested under the three-point flexural bending and repeated drop weight impact test, respectively. Because of the comparison between the impact and flexural energy absorption, the impact and flexural specimens must have the same dimension. In order to determine and evaluate the flexural strength of composite panels, 24 concrete slabs specimens (2 slabs from each composition) with dimensions of 300 mm × 400 mm and two thickness values of 25 and 50 mm, were cast and tested under flexural three-point bending and repeated drop weight impact. Details of prepared panels in this study are presented in Table 4 and Fig. 2. Panels were built in 12 models with different

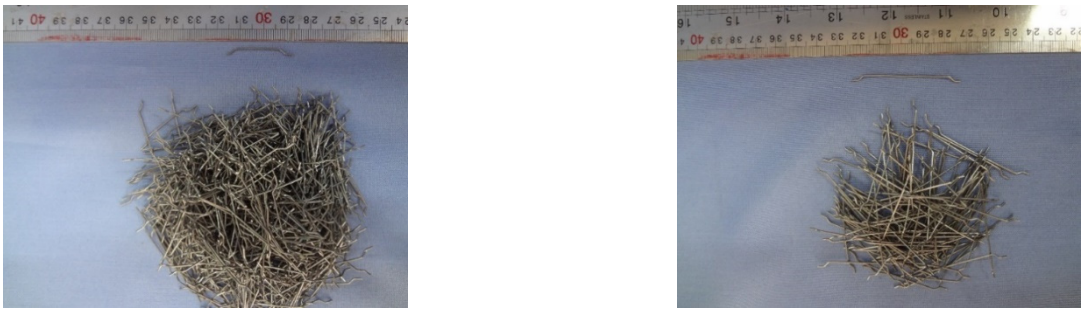

(a) Steel fiber 25 mm (b) Steel fiber 50 mm

Fig. 1 Steel fibers with different lengths of 25 and 50 mm

Table 3 Mixture proportions of self-compacting cementitious composite

Specimen designation	W/C	Wate (Kg/m^3)	Fly ash (Kg/m^3)	Cement (Kg/m^3)	Aggregates (Kg/m^3)	Fibers 50 m (vol-%)	Fibers 25 m (vol-%)	SP
Ref	0.37	453	180	750	1470	0	0	4.8
S5P1	0.37	453	180	750	1470	1	0	4.8
S2.5P1	0.37	453	180	750	1470	0	1	4.8
CSP0.5	0.37	453	180	750	1470	0.5	0.5	4.8
CS5_0.75	0.37	453	180	750	1470	0.75	0.25	4.8
CS5_0.25	0.37	453	180	750	1470	0.25	0.75	4.8

Table 4 Properties of composite panels with dimensions of 400 mm × 300 mm

Specimen No.	Specimen name	Panel depth (mm)	Fibers 50 mm (vol-%)	Fibers 25 mm (vol-%)
1	Ref_d3	30	0	0
2	S5P1d3	30	1	0
3	S2.5P13	30	0	1
4	CSP0.5d3	30	0.5	0.5
5	CS5_0.75d3	30	0.75	0.25
6	CS5_0.25d3	30	0.25	0.75
7	Ref_d5	50	0	0
8	S5P1d5	50	1	0
9	S2.5P1d5	50	0	1
10	CSP0.5d5	50	0.5	0.5
11	CS5_0.75d5	50	0.75	0.25
12	CS5_0.25d5	50	0.25	0.75

compositions of 25 mm and 50 mm steel fibers. Apart from the two control specimens (Ref), which lacked fibers, six specimens contained a mixture of 25 mm and 50 mm steel fibers, and the other four specimens had only 25 mm or 50 mm steel fibers. The mixing design was carried out in such a way that the volume fractions of steel fibers with various lengths remained constant at about 1 percent. All the panels had the same length and width. Also, their thickness was 30 mm and 50 mm. The specimens were tested under the flexural three-point bending test to determine the load-midspan displacement. To evaluate the impact performance of composite panels, a repeated drop weight test was conducted on composite specimens.

2.3 Test procedure

2.3.1 Mechanical properties

Compressive test

To determine the compressive strength of all mix compositions, eighteen cubic specimens with the dimension of 100 mm × 100 mm × 100 mm have been built and tested according to the ASTM C39. A digital compressive machine with a load cell capacity of 2000 kN has been used to determine the compressive strength with a loading rate of 0.3 MPa/s. The presented values for the compressive strength of all specimens are the average of three replicated cubic specimens.

Splitting tensile strength

To calculate the splitting tensile strength of all mix compositions, eighteen cylindrical specimens with a diameter of 100 mm and a height of 200 mm have been cast, cured, and tested in accordance with ASTM C496. A compressive digital test machine with a load cell capacity of 2000 kN has been used to determine the splitting tensile strength with a loading rate of 0.02 MPa/s. The reported values for splitting tensile strength of all specimens were determined by averaging the values of three replicated cylindrical specimens. Also, Eq. (1) has been used to calculate the splitting tensile strength

$$f_{sp} = \frac{2P}{\pi DL} \tag{1}$$

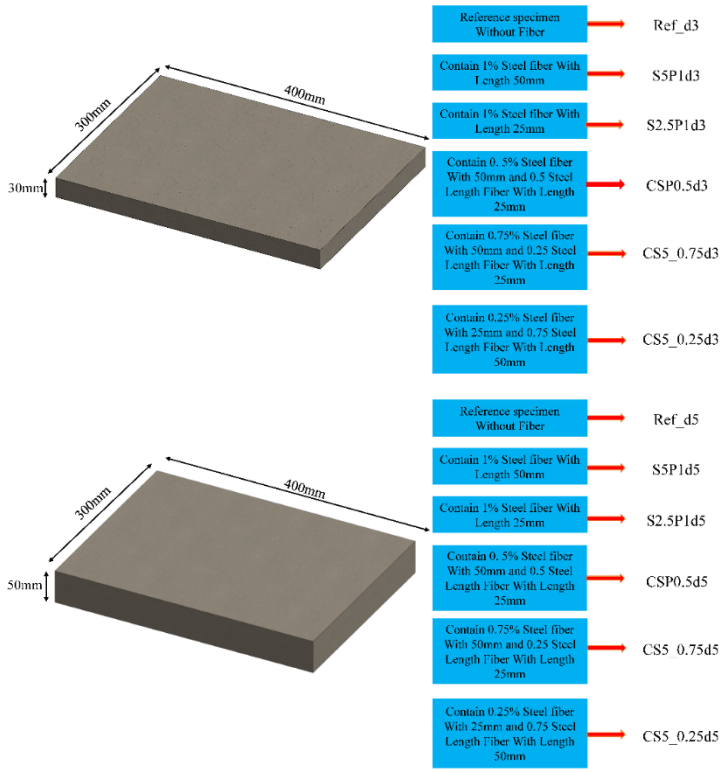

Fig. 2 Specification of composite panels

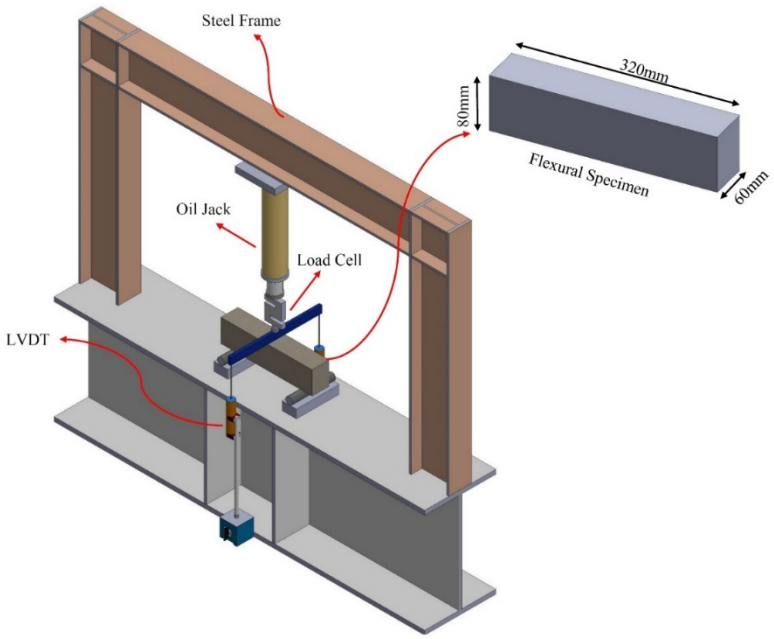

Fig. 3 Three-point flexural bending test setup

(a)

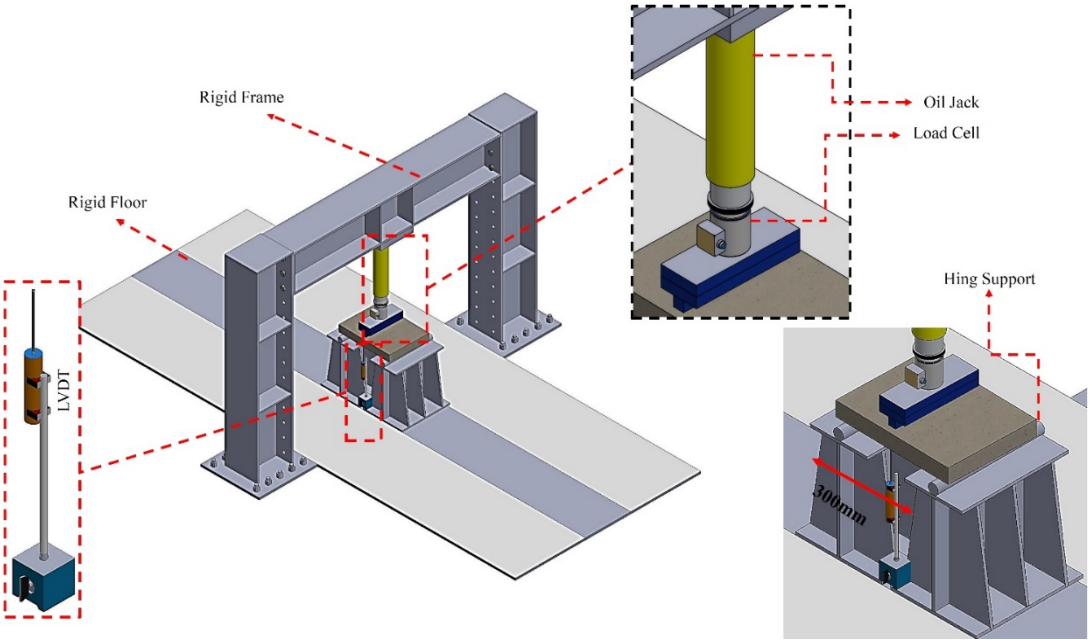

(b)

Fig. 4 Test overview of composite beam: (a) Experimental; (b) Schematic

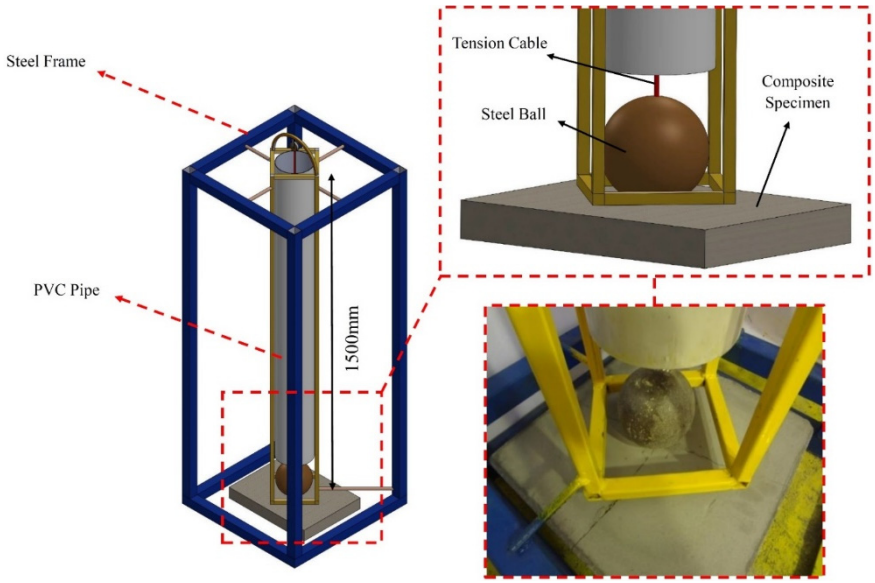

Fig. 5 Impact test setup

where, P is the maximum load, D is the diameter of the cylindrical specimen (equals 100 mm), and L is the length of the cylindrical specimen (equal to 200 mm).

Three-point bending test

Eighteen prismatic beams (320 mm × 80 mm × 60 mm) have been instrumented and tested to achieve the flexural performance of built-up composite beams. The testing procedure was in accordance with ASTM C293. A load cell with 50 kN capacity has been used to measure the force at the prismatic beams. In this study, a load rate of 1.0 MPa/min was applied at the top of the specimen continuously and without shock. The flexural strengths of the specimens have been determined from Eq. (2).

$$f_r = \frac{1.5PL}{bd^2} \quad (2)$$

where, P is the maximum load, L is the span length, and b and d are the width and height of the specimen, respectively. The flexural test setup is shown in Fig. 3. The results were determined by averaging the results of three tested beams.

2.3.2 Flexural performance of composite beams

As shown in Fig. 4, in order to perform the flexural test on the composite panels, a hydraulic jack and a load cell with a capacity of 200 kN have been utilized. Moreover, as can be seen from Fig. 4, by using two Linear Variable Differential Transformers (LVDT) at mid-span, the deflection of specimens can be measured. The exerted force with a rate of 1 mm/min was slowly applied to the composite panels, and the load-deflection curves were calculated for all specimens.

2.3.3 Repeated drop-weight impact performance

In the present study, a qualitative testing apparatus was used to evaluate the impact performance of composite panels (Moghadam *et al*. 2020, Naghibdehi *et al*. 2014). In this method, a steel ball with a weight of 5.6 Kg and diameters of 140 mm was repeatedly dropped on the top of composite panels until the failure was done on the top surface of the specimen. Because of the direct moving of the steel ball and its impact on the center of composite panels, a guide structure was utilized, which consists of a steel frame and a PVC pipe with a diameter of 150 mm. To reduce the friction force between the tension cable and the upper support, a pulley was used at the top of the guide structure. The details of the test setup for doing the impact test are shown in Fig. 5. In this test, the number of blows to occur the first visible crack (FC) and ultimate cracks (UC) was recorded. The criteria of this research to achieve failure mode was to observe splitting and crack propagation on the top of composite panels. Moreover, the absorbed energy of composite panels was determined from Eq. (3).

$$E_N = N \times W \times H \quad (3)$$

where N is the number of blows to create failure in the specimen, W is the weight of the steel ball, and H is the height of fall in mm.

3. Results and discussion

3.1 Mechanical properties

3.1.1 Compressive strength

To evaluate the compressive strength of 6 mixing designs, cubic specimens with dimensions of 100 mm × 100 mm × 100 mm were tested. Specimens were cast and tested according to the ASTM C39 standard. Results of the compressive test on cubic specimens are presented in Table 5. According to the results, mixing design S50P1 achieved the maximum compressive strength among the other mixing designs. Results of the compressive strength test indicated

Table 5 Compressive strength test result

Specimen No.	Specimen name	Compressive Strength (MPa)			Displacement at the failure of specimen (mm)
		Cubic (100 × 100 × 100)	Equivalent cylindrical strength (150 × 300)	Standard error	
1	Ref	68.10	58.91	0.75	1.42
2	S5P1	79.4	68.68	1.56	3.03
3	S2.5P1	70.12	60.65	1.18	2.12
4	CSP0.5	73.11	63.24	1.64	1.85
5	CS5_0.75	73.5	63.58	1.5	2.26
6	CS5_0.25	70.45	60.94	1.64	2.24

Table 6 Evaluation of splitting tensile and compressive strength relationship

Specimen name	Cubic compressive strength (MPa)	Split tensile strength (MPa)							
		Experimental (Standard error)	ACI Committee 318 (2014)	CEB-FIB (1991)	Oluokun *et al.* (1991)	Carino and Lew (1982)	Arioglu *et al.* (2006)	Lavanya and Jegan (2015)	Gardner (1990)
			$0.5(f_c')^{0.5}$	$0.3(f_c')^{0.66}$	$0.294(f_c')^{0.69}$	$0.272(f_c')^{0.71}$	$0.387(f_c')^{0.63}$	$0.249(f_c')^{0.772}$	$0.33(f_c')^{0.667}$
Ref	68.10	2.87 (0.08)	3.84	4.42	4.90	4.91	5.05	5.79	5.00
S5P1	79.40	7.86 (0.20)	4.14	4.89	5.44	5.48	5.56	6.52	5.54
S2.5P1	70.12	6.28 (0.16)	3.89	4.51	4.99	5.02	5.14	5.92	5.10
CSP0.5	73.11	7.15 (0.13)	3.98	4.63	5.14	5.17	5.28	6.12	5.25
CS5_0.75	73.50	7.25 (0.21)	3.99	4.65	5.16	5.19	5.29	6.14	5.26
CS5_0.25	70.45	6.99 (0.08)	3.9	4.52	5.01	5.03	5.15	5.94	5.12

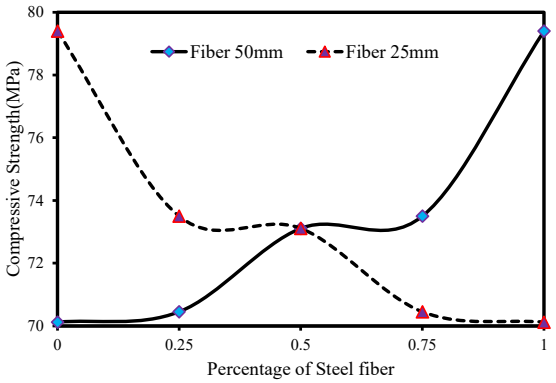

Fig. 6 Compressive strength versus percentage of steel fibers

a higher effect of fibers with 50 mm length on the value of compressive strength. In fact, the compressive strength increased with decreasing steel fiber content with 25 mm length in cubic specimens. As shown in Table 5, maximum displacement until the destruction moment belongs to the S5P1 group, and minimum displacement belongs to the non-fiber reference specimen. In addition, displacement at the moment of failure in the S5P1 group specimens with 1% volume fractions of steel fibers with 50 mm length is 43% higher than the displacement of S2.5P1 specimens. Likewise, displacement at the moment of failure in the CS5_0.75 mixing design is 1% higher in comparison with the CS5_0.25 mixing design. Variation of compressive strength of specimens versus fibers volume fractions is presented in Fig. 6. The positive effect of steel fibers with 50 mm length on compressive strength can also be observed in Fig. 6.

3.1.2 Splitting tensile strength

Splitting tensile strength was determined for cylindrical specimens casting based on the ASTM C496 standard. Concerning the results obtained from the splitting tensile tests in Table 6, the S5P1 group containing 1% volume fractions of steel fibers with 50 mm length has the highest tensile strength among the other specimens. As can be seen from the results, with increasing steel fiber content at 25 mm, the tensile strength decreased. According to splitting tensile test results, with increasing the length of fibers in the specimens, fiber-composite interaction would also increase, and therefore specimens' resistance to tensile forces might increase.

Based on Table 6, by incorporating 1% volume fractions of steel fibers with 50 mm length in S5P1 specimen, the tensile strength of this specimen in comparison with non-fiber reference specimen, and also in comparison with 1% volume fractions of steel fibers specimen with 25 mm length (S2.5P1) increased by 173% and 25%, respectively. Moreover, with increasing the volume fractions of steel fibers with 50 mm length, the displacement corresponding to the destruction point in the reference specimen increased from 0.42 mm to 8.72 mm in the S5P1 specimen. In addition, displacement corresponding to the failure point increased with increasing in the fibers' length, so that

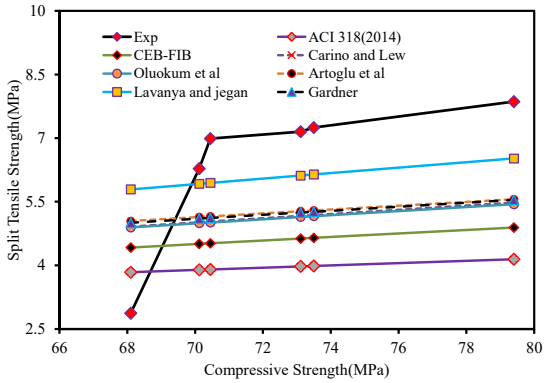

Fig. 7 Predicted splitting tensile strength of concrete from different models

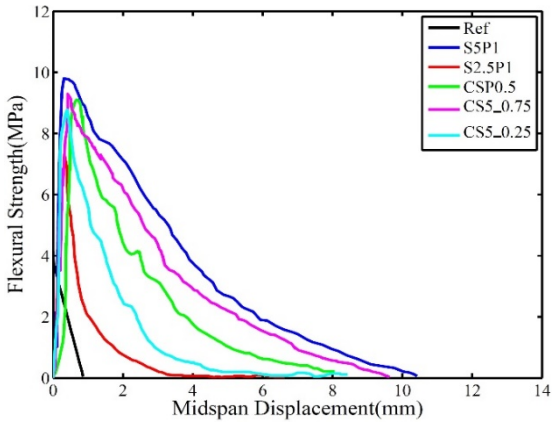

Fig. 8 Flexural strength versus midspan displacement

displacement in the S2.5P1 specimen increased from 4.47 mm to 8.72 mm in the S5P1 specimen.

In Fig. 7, a comparison was made between experimental and analytical results. As seen in Fig. 7, the difference between experimental values and prescribed values is relatively high. The reason for the difference is not to consider the effects of steel fibers in prescribed relations. Moreover, the minimum difference is between tensile strength values obtained from laboratory experiments and prescribed values obtained from the reference specimen.

3.1.3 Flexural three-point bending (FPB) tests

For the assessment of the effects of incorporating fibers in specimens on flexural strength, eighteen small bending beams with dimensions of 320 mm × 80 mm × 60 mm in 6 mixing designs were cast and tested under flexural three-point tests based on ASTM C78 standard. The flexural strength curve versus midspan displacement for all specimens is shown in Fig. 8.

In addition, flexural strength values calculated from the experimental results are presented in Table 7. According to Table 7, the maximum and minimum flexural strengths are corresponded to the S5P1 and reference mixing design, respectively. The amount of strength in the S2.5P1 mixing design is lower than that of the S50P1 mixing design. On the other hand, the amount of flexural strength in CS5_0.25 is lower in comparison with CS5_0.75.

In fact, with increasing shorter steel fibers content in mixing design in comparison with longer steel fibers content, the flexural strength of specimens reduces, as can be seen in Table 7; there is not much difference between the flexural strength values obtained from the experimental method for the reference specimens and prescribed values. However, by increasing the content of steel fibers, the difference between experimental and prescribed values increases significantly (Mastali *et al*. 2017).

In the S5P1 group, flexural strength is 9.8 MPa that in comparison with values calculated based on ACI 318-2002, ACI 318-2005, ACI 363, CEN, and IS standards are 48%, 56%, 21%, 41%, and 47% higher, respectively. In fact, the applications of fibers in the prescribed relations are not considered.

3.2 Flexural composite panel test results

In order to investigate the flexural behavior of self-compact composites, twenty-four slabs in 12 different designs were cast and tested. In this study, specimens were tested under concentrated loads at mid-span. Prepared panels had two thickness values of 30 mm and 50 mm, 400 mm length and 300 mm width.

3.2.1 Load - displacement behavior

The number of tested specimens was twelve, which are arranged as the following: two of them were non-fiber

Table 7 Evaluation of flexural and compressive strength relationship

Specimen name	Cubic compressive strength (MPa)	Split tensile strength (MPa)				
		Experimental (Standard error)	ACI Committee 318 (2002)	ACI Committee 318 (2005)	ACI Committee 363 (1992)	Indian code IS (2000)
			$0.62(f_c^{'})^{0.5}$	$0.517(f_c^{'})^{0.5}$	$0.94(f_c^{'})^{0.5}$	$0.626(f_c^{'})^{0.5}$
Ref	68.10	4.12 (0.07)	4.76	3.97	7.21	4.8
S5P1	79.40	9.8 (0.16)	5.14	4.28	7.79	5.19
S2.5P1	70.12	7.32 (0.10)	4.83	4.03	7.32	4.48
CSP0.5	73.11	9.1 (0.20)	4.93	4.11	7.48	4.98
CS5_0.75	73.50	9.29 (0.07)	4.94	4.12	7.5	4.99
CS5_0.25	70.45	8.77 (0.15)	4.84	4.04	7.34	4.89

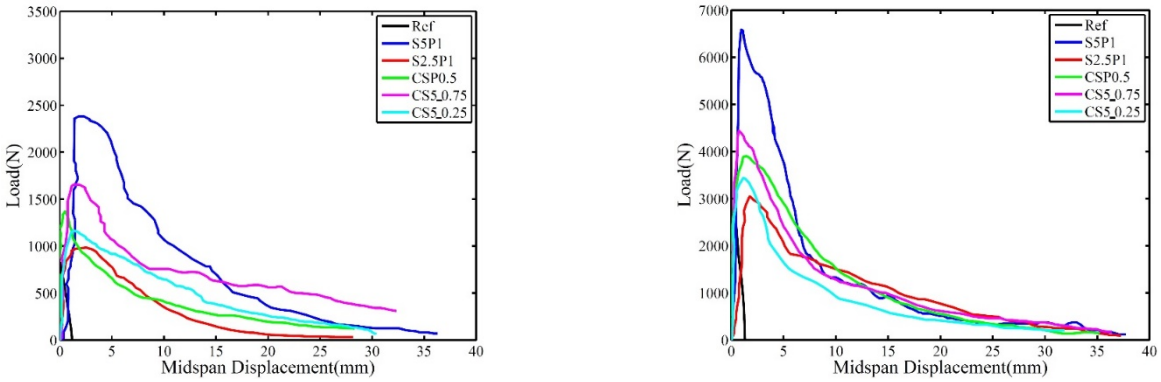

(a) (b)

Fig. 9 Load-displacement curve of composite panels with (a) 30 mm depth; (b) 50 mm depth

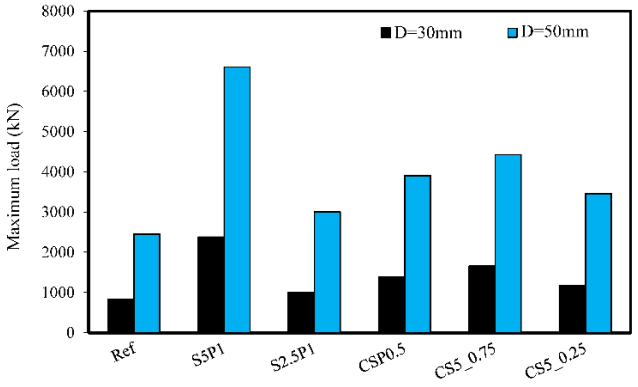

Fig. 10 Column diagram of maximum load for composite panels

specimens as the control sample, six of them were mixed-fibers specimens with two lengths of 50 and 25 mm, and four specimens containing fibers with 25 mm or 50 mm length alone. All the specimens were considered as single-layer samples tested under Flexural three-point bending (FPB) tests. The load-displacement diagrams are presented in Fig. 9. Based on the results, the flexural strength increased in slabs containing 50 mm steel fibers. In fact, by increasing steel fibers content, the amount of flexural strength increased. In slabs with 50 mm thickness, the S5P1_d5 specimen had the maximum flexural capacity, among others. The flexural capacity of the S5P1_d5 specimen was 44% higher than that of the Ref_d5 specimen. Moreover, using 1% volume fractions of steel fibers with 50 mm thickness led to increasing the strength by 44%, compared to the S2.5P1_d5 specimen. A comparison of slabs with the same fiber contents, but with a different layout, demonstrated how the layout of the fibers had significant effects on the flexural behavior of the specimens. Therefore, longer fiber's layouts resulted in a significant improvement in the slabs' flexural strengths. The column diagram of maximum loading capacities of composites slabs is presented in Fig. 10; as shown in Fig. 10, the effect of thickness on the loading capacity of specimens in the two groups is significant. In non-fiber specimens, with a decrease of 20 mm in the thickness of slab composites, the loading capacities were reduced from 2438.36 to 820.16. Additionally, the maximum average of loading capacities of composite slabs with 50 mm thickness was about 3966 kN, 2.48 times more than the loading capacities of the same specimens with 30 mm thickness. In specimens with 50 mm thickness, the maximum and minimum values of the final displacement of steel fibers were 31.81 mm and 37.71 mm, respectively. Moreover, in slabs with 30 mm thickness, the maximum and minimum values of the final displacements of steel fibers were 28.18 and 36.06, respectively. In other words, in comparison with the same values in 30 mm slabs, the maximum and minimum displacements in 50 mm slabs were 5% and 13% higher, respectively.

3.2.2 Flexural ductility

The difference between the slabs' ductility is presented in Table 8 and Fig. 11. Obtained results of the experiments demonstrated that non-fiber specimens lacked ductility, and therefore they rapidly failed after the occurrence of the first crack. Moreover, findings indicated that steel fibers led to the formation of cracks stitching effect, preventing crack propagation. By incorporating fibers, the slabs' resistance and ductility increased significantly. On the other hand, increasing the use of longer fibers led to an improvement in the ductility of the specimens. However, comparing long and short fibers, incorporating short fibers led to a reduction of ductility. Furthermore, when the thickness increased from 30 mm to 50 mm, the ductility coefficient of specimens increased as well. In slabs with 30 mm thickness, the maximum ductility coefficient of 27.32 belonged to the S5P1_d3 group. The ductility coefficient for the S5P1_d3 group was 47% higher than that for the S25P1-d30 group with 1% steel fiber content. Fig. 12 presents changes in the ductility coefficients based on fibers with two lengths of 25 mm and 50 mm. As shown in Fig. 12, the ductility coefficient increases by increasing steel fibers content with 50 mm length. The range of changes of ductility coefficient for slabs with 30 mm thickness and for slabs with 50mm thickness was 8.66 mm and 10.75 mm, respectively. In other words, the range of changes in ductility coefficient for the slabs with 50 mm thickness was 24% higher than those for the slabs with 30 mm thickness. Changes in ductility coefficient were reduced with increasing the fiber content. Predicted linear relationships for the calculation of the

Table 8 Ductility factor of composite slab specimens

Specimen name	Max load (N)	Δ_y (mm)	Δ_U (mm)	Ductility		
				Experimental	Proposed equation	Error (%)
Ref_d3	820.16	0.17	1.18	6.95	--	--
S5P1_d3	2379.70	1.32	36.06	27.32	28.33	3.69
S2.5P1_d3	984.33	1.51	28.18	18.66	19.36	3.75
CSP0.5_d3	1370.03	1.11	28.33	25.52	23.84	-6.57
CS5_0.75d3	1650.02	1.21	31.96	26.41	26.09	-1.23
CS5_0.25d3	1165.16	1.41	30.05	21.31	21.60	1.37
Ref_d5	2438.36	0.37	1.32	3.57	--	--
S5P1_d5	6585.40	1.11	37.71	33.97	34.56	1.73
S2.5P1_d5	3023.75	1.60	37.15	23.22	23.48	1.12
CSP0.5_d5	3900.30	1.21	35.25	29.13	29.02	-0.38
CS5_0.75d5	4439.00	1.11	36.05	32.48	31.79	-2.13
CS5_0.25d5	3413.82	1.21	31.81	26.29	26.25	-0.16

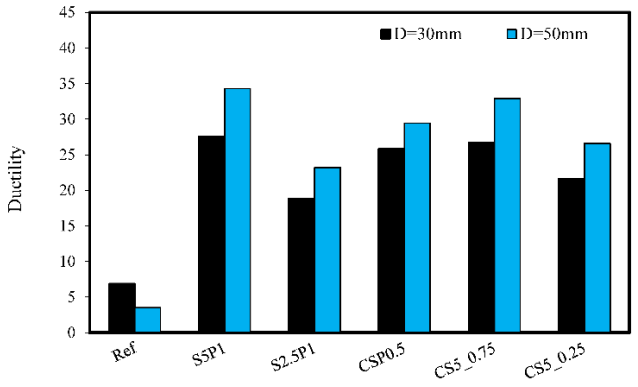

Fig. 11 Column diagram of flexural ductility

ductility coefficient of slabs are presented in Fig. 12. A comparison between experimental ductility coefficients and the same values predicted by the analytical equations is also shown in Table 8. As shown in Table 8, the maximum and minimum differences between analytical and experimental values belong to the CSP0.5_d3 and CSP0.5_d5 groups, respectively.

3.2.3 Flexural absorbed energy

According to Table 9, the energy absorption of specimens was calculated by measuring the area of the load-displacement curve. Also, the composite panels with 50 mm thickness, including 1% fiber (with a length of 50 mm), had the maximum energy absorption, and it was 24.7 times more than the Ref_d5 group. In comparison between the panels with different thicknesses, the maximum energy absorption of the 50 mm panels was about 49.19 KJ, which was 88% higher than the maximum absorbed energy of the slabs with 30 mm thickness.

In the group, including slabs with 30 mm thickness, the maximum absorbed energy was 26.16 KJ for the S50P1-d30 group. Regarding the absorbed energy of specimens, the mean value of the absorbed energy of specimens with 50 mm thickness was 33.35 KJ. The mean value of the energy absorbed by the specimens with 50 mm thickness was 136% higher than the mean value of energy absorbed by specimens with 30 mm thickness. Moreover, the amount of absorbed energy variations of fiber slabs with 30 mm and 50 mm thickness were 20.41 and 17.14 KJ, respectively. However, in both groups, non-fiber slabs (Ref_d3 and Ref_d5) rapidly failed. The absorbed energy of the non-

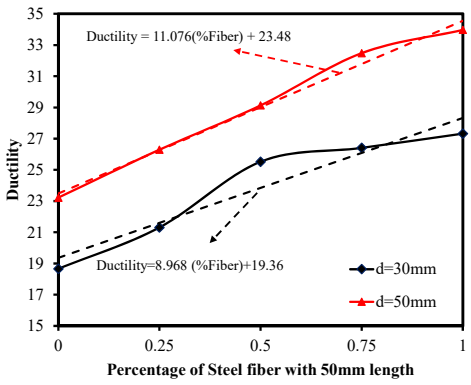

(a) 50 mm steel fiber

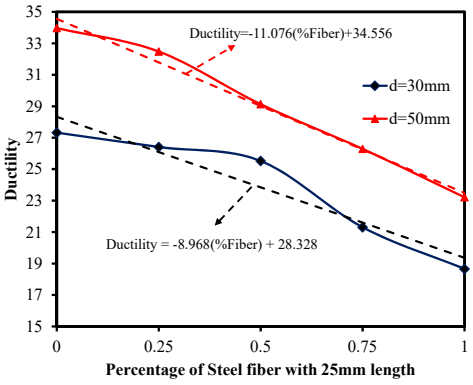

(b) 25 mm steel fiber

Fig. 12 Changes in ductility factor versus steel fiber percentage

Table 9 Absorbed energy of flexural composite slab specimens

Specimen	Absorbed energy		
	Experimental	Proposed equation	Error (%)
Ref_d5	1.99	--	--
S5P1_d5	49.19	49.14	-0.10
S2.5P1_d5	37.23	37.23	0.00
CSP0.5_d5	41.52	41.51	-0.02
CS5_0.75d5	41.41	41.38	-0.06
CS5_0.25d5	28.78	28.78	-0.01
Ref_d3	0.51	--	--
S5P1_d3	26.16	26.19	0.09
S2.5P1_d3	9.02	9.03	0.06
CSP0.5_d3	11.27	11.27	0.03
CS5_0.75d3	22.92	22.93	0.05
CS5_0.25d3	14.89	14.89	0.00

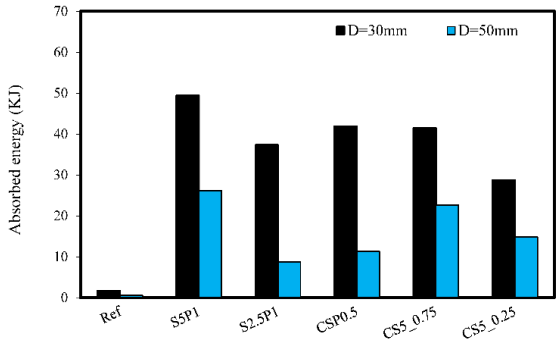

Fig. 13 Column diagram for absorbed energy of flexural composite slab specimens

fiber reference specimen for slabs with 50 mm and 30 mm thickness were 1.99 and 0.51 KJ, respectively. In Fig. 13, the column diagram of energy absorption is shown. As noted in Fig. 13, the difference between the energy absorbed by non-fiber specimens and that by the fibrous specimens was very high. Moreover, a diagram of the absorbed energy variation of specimens based on fiber content with thicknesses of 25 mm and 50 mm has been presented in Fig. 14.

As shown in Fig. 14, in specimens with a thickness of 50 mm, with the increase in fiber content from 0 to 1%, the amount of energy absorption approximately increases. Likewise, by increasing fiber content from 0 to 1% in fiber with 30 mm thickness, the amount of energy absorption approximately increases. Additionally, by increasing the fibers content with a length of 25 mm, the amount of energy absorption followed an approximately decreasing trend. These decreasing trends for both groups with two thicknesses of 30 mm and 50 mm were the same. Moreover, in Fig. 14, an equation is given to calculate the amount of energy absorption of specimens containing fibers with lengths of 50 mm and 25 mm. The percentage of differences between the absorbed energy of specimens obtained from laboratory tests and analytical relations are presented in Table 9. As shown in Table 9, there is no significant difference between the experimental and analytical values (less than 0.1%).

3.2.4 Flexural toughness

The flexural toughness of specimens for the equivalent displacement (L/150) and flexural strength coefficient based on ASTM C1609 are presented in Table 10. Until 2006, researchers used to calculate flexural strength based on the ASTM C1018 standard. Based on this standard, the displacement corresponding to the first crack occurrence must be determined. Because of the difficulties in the exact determination of parameters, this standard was abolished after 2006. In recent years, the ASTM C1609 standard has been used to determine flexural toughness as an alternative to the ASTM C1018 standard. In this study, both ASTM C1018 and ASTM C1609 standards were used to determine flexural toughness. Data were analyzed using both methods. In order to determine the flexural toughness by ASTM C1018 standard, the parameters I5, I10, I15 and I20 were calculated according to Fig. 15. Also, as can be seen in Table 10, the non-fiber groups represent no behavior after cracking. As can be observed in Fig. 16, the CS5_0.25 and

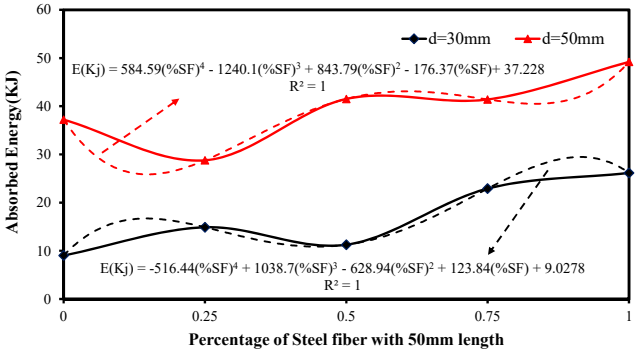

(a) 50 mm steel fiber

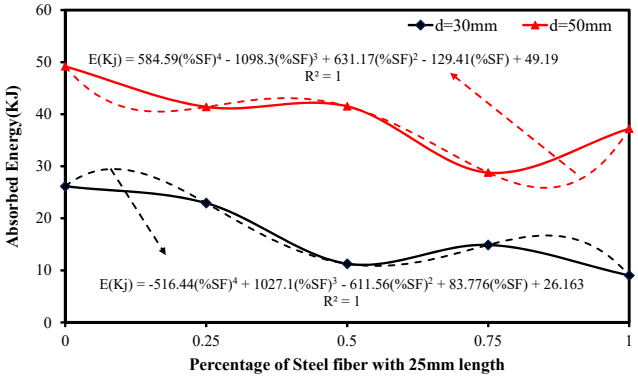

(b) 25 mm steel fiber

Fig. 14 Changes in absorbed energy versus steel fiber percentage

Table 10 Flexural toughness factors and indices of composite slabs

Specimen	According to ASTM C1018				According to ASTM C1609		
	I_5	I_{10}	I_{15}	I_{20}	$\mathbf{T_{150}^D}$(Kj)	Modulus of Rupture (MPa)	$\mathbf{R_{T,150}^D}$
Ref_d3	3.24	4.90	0.00	0.00	0.00	1.59	0.00
S5P1_d3	5.43	10.55	16.43	19.34	2.78	4.63	0.33
S2.5P1_d3	3.61	5.82	7.65	8.13	1.89	1.91	0.55
CSP0.5_d3	4.13	6.42	9.40	11.33	2.57	2.66	0.54
CS5_0.75d3	4.07	6.77	10.49	13.59	3.11	3.21	0.54
CS5_0.25d3	3.42	5.93	9.19	10.91	2.29	2.27	0.56
Ref_d5	3.24	0.00	0.00	0.00	0.00	1.71	0.00
S5P1_d5	4.66	8.02	10.86	12.50	11.31	4.61	0.49
S2.5P1_d5	4.69	7.76	12.07	14.43	4.42	2.12	0.42
CSP0.5_d5	3.34	5.57	8.15	9.49	8.19	2.73	0.60
CS5_0.75d5	3.94	6.87	10.56	12.85	8.75	3.11	0.56
CS5_0.25d5	3.38	5.11	7.25	8.49	6.91	2.39	0.58

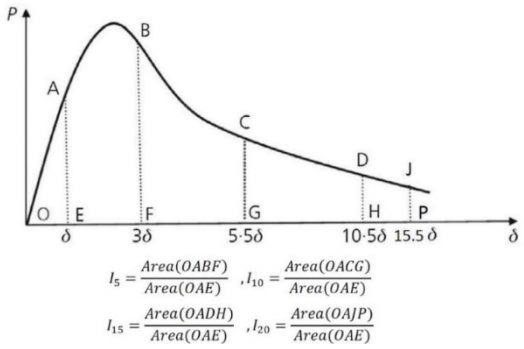

Fig. 15 Definition of flexural toughness indices based on ASTM C1018

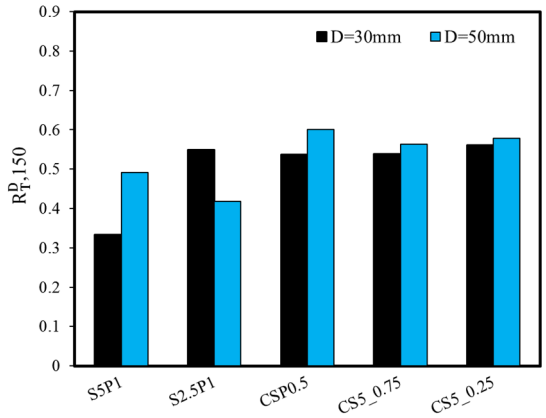

Fig. 16 Column diagram for flexural toughness indices ASTM C1018

CSP0.5 groups have the highest flexural coefficients in slabs with 30 mm thickness and slabs with 50 mm, respectively.

3.3 Impact results

3.3.1 First crack strength

The impact test was carried out on 12 specimens (two specimens from each group) with two different thicknesses of 30 mm and 50 mm. The number of blows to occur in the first visible crack was recorded from the impact test, and these results are shown in Table 11. Also, the column diagram for the first crack strength of panels is depicted in Fig. 17. As shown in Fig. 17, the first crack strength of the reference specimen in panels with 30 mm thickness was six blows. On the other hand, the first crack strength of the panels was strongly increased by adding steel fiber. The maximum and minimum values of the first crack strength in panels with 30 mm thickness belong to the Ref and S5P1_d3, respectively. This similar behavior is observed in panels with 50mm thickness. The first crack strength was approximately increased by about 30% with increasing the thickness of panels from 30 mm to 50 mm. Also, the maximum first crack strength in panels with 30 mm was 120 blows, which belongs to the S5P1_d3 group. Moreover, in panels with 50 mm thickness, the maximum first crack strength was 150 blows. In fact, due to the increase in panels thickness from 30 to 50 mm, the first crack strength was increased by 25%, and the minimum first crack strength in fibrous panels belongs to S2.5P1_d3. This first crack strength of panels with 30 and 50 mm thicknesses were 95 and 123 blows, respectively. Based on the results, the maximum difference of the first crack strength in fibrous panels was 25 and 28 blows for specimens with 30 mm and 50 mm thickness, respectively.

According to Fig. 18, in all panels, by increasing the content of 25 mm steel fiber, the first crack strength was decreased in comparison with fibers with a length of 50 mm. Also, the first crack strength was increased by increasing of fiber percentage with a length of 50 mm. As can be seen in Fig. 18, the variations of first crack strength versus fiber percentage, are approximately in linear form.

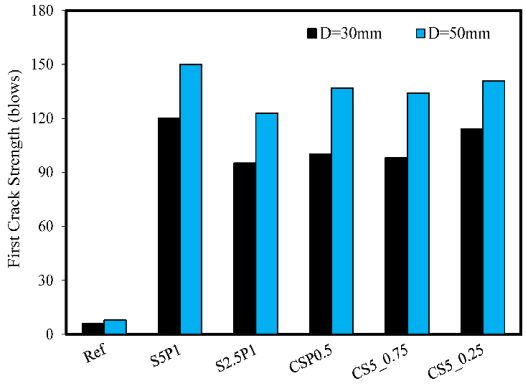

Fig. 17 First crack strength of composite panels

The slope of these curves was descending by increasing the contents of 25 mm steel fiber, whereas it was ascending with increasing contents of 50 mm steel fiber. As can be expected, these variations in curves slope illustrate the more effects of 50 mm steel fiber on the first crack strength of composite panels. In Fig. 18, the proposed Equations to determine the first crack strength of composite panels are depicted in the form of fiber percentage.

3.3.2 Failure strength

As can be seen from Table 11, the number of blows recorded to occur in failure mode in the composite panel is presented. In this research, the main ultimate failure criterion for composite panels was the splitting of panels into several pieces or cracks propagation on the surface of panels. According to Fig. 19, the impact resistance of reference specimens had low values because of the non-presence of steel fibers in composite panels. Also, the failure strength of panels with 30 mm and 50 mm thickness was 11 and 14 blows, respectively. In comparison with composite panels containing steel fiber, the failure strength of non-fibrous panels was very low. In composite panels with 30 mm thickness, the maximum and minimum failure strength belonged to S5P1, and S2.5P1 with values of 401, and 207 blows, respectively. Also, in the 50mm panels, the maximum and minimum failure strength belongs to S5P1, and S2.5P1 with values of 560, and 360 blows, respectively. The highest failure strength at 30 mm panels was 401 blows

Table 11 Repeated impact test results

Specimen name	First crack strength (Blows)	Ultimate strength (Blows)	PINPB (%)
Ref_d3	6	11	83
S5P1_d3	120	401	234
S2.5P1_d3	95	270	184
CSP0.5_d3	100	312	212
CS5_0.75d3	98	301	207
CS5_0.25d3	114	366	221
Ref_d5	8	14	75
S5P1_d5	150	560	273
S2.5P1_d5	123	360	193
CSP0.5_d5	137	451	229
CS5_0.75d5	134	439	228
CS5_0.25d5	141	472	235

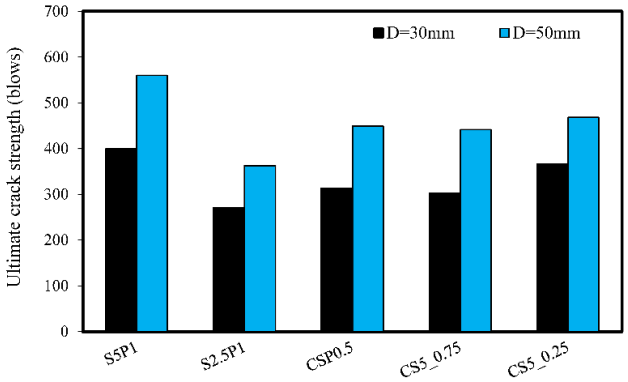

Fig. 19 Column diagram for ultimate crack strength of composite panels

which were 30% lower than the maximum failure strength of panels with 50 mm thickness. With regard to the results, it can be observed which values of failure strength in the CS5P_0.75 group were more than in the CS5_0.25 group. Moreover, in composite panels with 30 and 50 mm thickness, the ultimate strength of the CS5P_0.75 group was 366 and 472 blows which indicated 22% and 8%, increasing

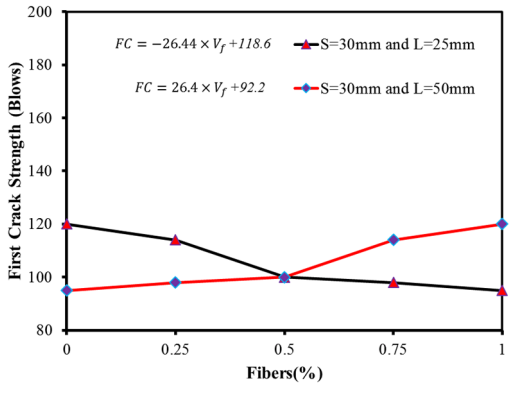

(a) Composite panels with 30 mm thickness

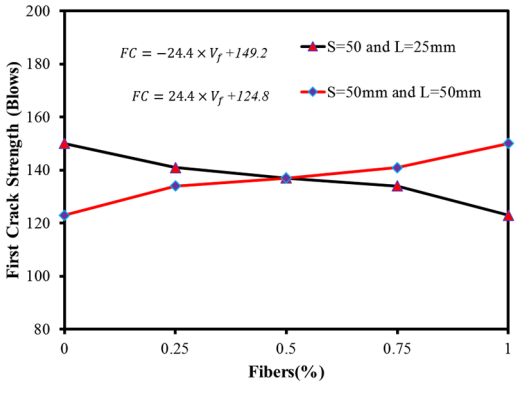

(b) Composite panels with 50 mm thickness

Fig. 18 The changes in first crack strength versus fiber percentage

Fig. 20 Failure mode of composite panels

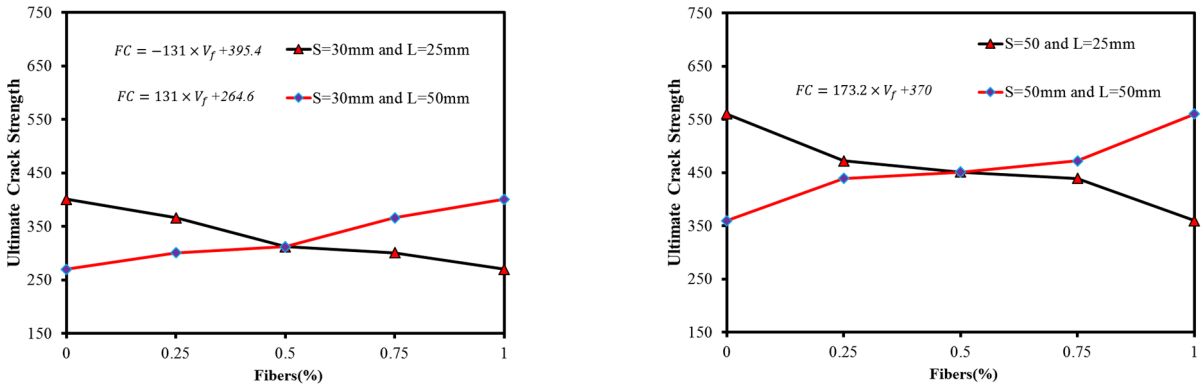

(a) Composite panels with 30 mm thickness

(b) Composite panels with 50 mm thickness

Fig. 21 The changes in first crack strength versus fiber percentage

respect to the CS5_0.25 group. Based on the impact result, it can be concluded that increasing of steel fiber with longer length in composite panels resulted in an increase of the impact resistance of panels. In Fig. 20, the performed test to calculate the impact resistance of specimens is shown.

3.3.3 Absorbed energy

The absorbed energy of composite panels was calculated from Eq. (3) and is shown in Table 12 in terms of KJ. The results show that there was a considerable difference between the absorbed energy of fibrous and non-fibrous composite panels. Due to the high integrity and sewing of crack by steel fibers, the absorbed energy of fibrous specimens was increased compared to the non-fibrous panels.

Moreover, the length of steel fibers was very effective in the absorbed energy of panels. Also, in accordance with the experimental results, the absorbed energy was increased by increasing the utilization of 50 mm steel fibers. The maximum absorbed energy of composite panels belongs to the S5P1_d5 with a value of 47.79 KJ, which was 56% more than the S2.5P1_d3 group, and the minimum absorbed energy among all specimens belongs to S25P1_d3. The average absorbed energy of composite panels with thicknesses of 30 mm and 50 mm was 23.63 KJ and 32.66 KJ, respectively. In fact, the absorbed energy of composite panels with a thickness of 50 mm was 38% more than the composite panels with 30 mm thickness. In Table 12, the calculated absorbed energy for specimens extracted from experimental data, and the proposed equation is presented. Based on these results, the minimum and maximum errors of predicted data from the proposed equation are 0.1% and 16.1%. The proposed Eqs. (4) and (5) calculate the absorbed energy of composite panels with 30 mm and 50 mm thicknesses, respectively. The parameter $f_c^{'}$ in these equations is the cylindrical compressive strength of

Table 12 Calculated absorbed energy extracted from experimental and proposed equations

Specimen ID	Absorbed energy (KJ)		Absolute error (%)
	Experimental	Proposed equation	
Ref_d3	0.94	--	--
S5P1_d3	34.22	29.88	12.7
S2.5P1_d3	23.04	22.74	1.3
CSP0.5_d3	26.63	28.68	7.7
CS5_0.75d3	25.69	29.81	16.1
CS5_0.25d3	31.24	28.96	7.3
Ref_d5	1.19	--	--
S5P1_d5	47.79	42.59	10.9
S2.5P1_d5	30.72	30.70	0.1
CSP0.5_d5	38.49	39.32	2.1
CS5_0.75d5	37.47	42.59	13.7
CS5_0.25d5	40.28	39.96	0.8

composite panels in MPa.

$$E = 27.843f_c^{'} - 0.221(f_c^{'})^2 - 847.07 \quad (4)$$

$$E = 54.489f_c^{'} - 0.429(f_c^{'})^2 - 1685.2 \quad (5)$$

4. Conclusions

The results obtained from this experimental investigation show that six base mixing designs were carefully selected, and also, the performed impact and flexural tests showed significant experimental information; thus, the following results can be concluded:

(1) According to the experimental results, the use of steel fiber led to reducing concrete consistency, and this effect was increased with fibers length. In fact, by using longer fibers, the consistency of self-compacting composites decreased.
(2) Based on the experimental results, the maximum compressive strength belongs to the S50P1 group, and utilizing steel fiber with longer length was caused to increase compressive strength. Moreover, due to adding 25 mm steel fiber into the mixtures, the compressive strength was increased.
(3) Conforming with the experimental results, adding 25 mm steel fiber into mixtures led to reducing in the flexural strength of prismatic specimens. Also, the results of non-fiber specimens were similar, and adding the fibers to the mixture caused differences between the experimental and code-calculated values. In the S0p1 group, the flexural strength value was 9.8 MPa, which was 48%, 56%, 21%, 41%, and 47% higher than the values of those obtained based on ACI 318-2002, ACI 318-2005, ACI 363, CEN and IS standards, respectively.
(4) The presented results of the composite slab flexural test show that in specimens with 30 mm and 50 mm thickness, the lowest capacity belonged to the non-fiber reference specimens. The maximum and minimum loading capacities regarding specimens with 30 mm thickness belonged to Ref and S50P1 specimens, respectively. Moreover, by increasing in panels' thickness from 30 mm to 50 mm, the flexural strength increased about 197%.
(5) Based on the results, it was concluded that there was a significant difference between the absorbed energy of non-fiber slabs and fibrous slabs, and this behavior can be relevant to increasing slab integrity by using more fibers. The maximum energy absorption by the value of 49.19 KJ belonged to the slabs with 50 mm thickness, which was 88% higher than the maximum absorbed energy of the slabs with 30 mm thickness. The mean value of energy absorbed by the composite panels of 50 mm thick was 136% higher as compared to the value of composite panels of 30 mm thick.
(6) Furthermore, the impact test results were shown a significant increase in the specimens' impact strength with an increase in the fiber's length. Also, adding fibers to the composition led to growth in the energy absorption of composite panels. Moreover, the maximum impact absorbed energy was 47.79 KJ which was 69% more than the average value.

References

ACI Committee 318 (2014), Building Code Requirements for Structural Concrete (ACI 318-14) and Commentary (318R-14), American Concrete Institute, Farmington Hills, MI, USA.

Afzali-Naniz, O. and Mazloom, M. (2019), "Fracture behavior of self-compacting semi-lightweight concrete containing nano-silica", *Adv. Struct. Eng.*, **22**(10), 2264-2277. https://doi.org/10.1177/1369433219837426

Ahmadi, M., Kheyroddin, A., Dalvand, A. and Kioumarsi, M. (2020), "New empirical approach for determining nominal shear capacity of steel fiber reinforced concrete beams", *Constr. Build. Mater.*, **234**, p. 117293. https://doi.org/10.1016/j.conbuildmat.2019.117293

Arioglu, N., Girgin, Z.C. and Arioglu, E. (2006), "Evaluation of ratio between splitting tensile strength and compressive strength for concretes up to 120 MPa and its application in strength criterion", *ACI Mater. J.*, **103**(1), 18-24.

Aslani, F. and Nejadi, S. (2012), "Bond Behavior of Reinforcement in Conventional and Self-Compacting Concrete", *Adv. Struct. Eng.*, **15**(2), 2033-2051. https://doi.org/10.1260/1369-4332.15.12.2033

ASTM C39 / C39M-09a (2009), Standard Test Method for Compressive Strength of Cylindrical Concrete Specimens, ASTM International; West Conshohocken, PA, USA. www.astm.org, https://doi.org/10.1520/C0039_C0039M-09A

ASTM C39 / C39M-21 (2021), Standard Test Method for Compressive Strength of Cylindrical Concrete Specimens, ASTM International, West Conshohocken, PA, USA. www.astm.org, https://doi.org/10.1520/C0039_C0039M-21

ASTM C496 / C496M-04 (2004), Standard Test Method for Splitting Tensile Strength of Cylindrical Concrete Specimens, ASTM International; West Conshohocken, PA, USA. www.astm.org, https://doi.org/10.1520/C0496_C0496M-04

ASTM C496 / C496M-17 (2017), Standard Test Method for Splitting Tensile Strength of Cylindrical Concrete Specimens, ASTM International; West Conshohocken, PA, USA. www.astm.org, https://doi.org/10.1520/C0496_C0496M-17

ASTM C1609 / C1609M-05 (2005), Standard Test Method for Flexural Performance of Fiber-Reinforced Concrete (Using Beam With Third-Point Loading), ASTM International; West Conshohocken, PA, USA. www.astm.org, https://doi.org/10.1520/C1609_C1609M-05

ASTM C1609 / C1609M-19 (2019), Standard Test Method for Flexural Performance of Fiber-Reinforced Concrete (Using Beam With Third-Point Loading), ASTM International; West Conshohocken, PA, USA. www.astm.org, https://doi.org/10.1520/C1609_C1609M-19

Banthia, N. and Sappakittipakorn, M. (2007), "Toughness enhancement in steel fiber reinforced concrete through fiber hybridization", *Cement Concrete Res.*, **37**(9), 1366-1372. https://doi.org/10.1016/j.cemconres.2007.05.005

Benyamina, S., Menadi, B., Bernard, S.K. and Kenai, S. (2019), "Performance of self-compacting concrete with manufactured crushed sand", *Adv. Concrete Constr., Int. J.*, **7**(2), 87-96. https://doi.org/10.12989/acc.2019.7.2.087

Carino, N.J. and Lew, H.S. (1982), "Re-examination of the relation between splitting tensile and compressive strength of normal weight concrete", *ACI Mater. J.*, **79**(3), 214-219.

CEB-FIP Model Code for Concrete Structures (1991), Evaluation of the Time Dependent Behaviour of Concrete, Bulletin

d'Information No. 199, Comite European du Béton/Fédération Internationale de la Precontrainte, Lausanne, Switzerland.

Chan, C., Yu, T. and Zhang, S. (2018), "Compressive behaviour of square fibre-reinforced polymer–concrete–steel hybrid multi-tube concrete columns", *Adv. Struct. Eng.*, **21**(8), 1162-1172. https://doi.org/10.1177/1369433217732499

Dalvand, A. and Ahmadi, M. (2021), "Impact failure mechanism and mechanical characteristics of steel fiber reinforced self-compacting cementitious composites containing silica fume", *Eng. Sci. Technol.*, **24**(3), 736-748. https://doi.org/10.1016/j.jestch.2020.12.016

Djelloul, O.K., Menadi, B., Wardeh, G. and Kenai, S. (2018), "Performance of self-compacting concrete made with coarse and fine recycled concrete aggregates and ground granulated blast-furnace slag", *Adv. Concrete Constr., Int. J.*, **6**(2), 103-121. https://doi.org/10.12989/acc.2018.6.2.103

Facconi, L., Minelli, F. and Plizzari, G. (2016), "Steel fiber reinforced self-compacting concrete thin slabs – Experimental study and verification against Model Code 2010 provisions", *Eng. Struct.*, **122**(1), 226-237. https://doi.org/10.1016/j.engstruct.2016.04.030

Gardner, N.J. (1990), "Effect of Temperature on the Early-Age Properties of Type I, Type III, and Type I/Fly Ash Concretes", ACI Materials Journal, 87(1), 68-78.

Huang, B.-T., Wu, J.-Q., Yu, J., Dai, J.-G., Leung, C.K.Y. and Li, V.C. (2021), "Seawater sea-sand engineered/strain-hardening cementitious composites (ECC/SHCC): Assessment and modeling of crack characteristics", *Cement Concrete Res.*, **140**, 106292. https://doi.org/10.1016/j.cemconres.2020.106292

Karanth, S.S., Ghorpade, V.G. and Rao, H.S. (2017), "Shear and impact strength of waste plastic fibre reinforced concrete", *Adv. Concrete Constr., Int. J.*, **5**(2), 173-182. https://doi.org/10.12989/acc.2017.5.2.173

Karihaloo, B.L. and Wang, J. (1997), "Micromechanical modelling of strain hardening and tension softening in cementitious composites", *Computat. Mech.*, **19**, 453-462. https://doi.org/10.1007/s004660050193

Karimipour, A., Ghalehnovi, M., de Brito, J. and Attari, M. (2020), "The effect of polypropylene fibres on the compressive strength, impact and heat resistance of self-compacting concrete", *Structures*, **25**, 72-87. https://doi.org/10.1016/j.istruc.2020.02.022

Kim, S., Jeong, S.Y. and Kang, T.H.K. (2019), "Design of small impact test device for concrete panels subject to high speed collision", *Adv. Concrete Constr., Int. J.*, **7**(1), 23-30. https://doi.org/10.12989/acc.2019.7.1.023

Kong, H.-J., Bike, S.G. and Li, V.C. (2003), "Development of a self-consolidating engineered cementitious composite employing electrosteric dispersion/stabilization", *Cement Concrete Compos.*, **25**(3), 301-309. https://doi.org/10.1016/S0958-9465(02)00057-4

Lavanya, G. and Jegan, J. (2015), "Evaluation of relationship between split tensile strength and compressive strength for geopolymer concrete of varying grades and molarity", *Int. J. Appl. Eng. Res.*, **10**(15), 35523-35527.

Lenka, S. and Panda, K.C. (2017), "Effect of metakaolin on the properties of conventional and self compacting concrete", *Adv. Concrete Constr., Int. J.*, **5**(1), 31-48. https://doi.org/10.12989/acc.2017.5.1.31

Lepech, M.D., Li, V.C., Robertson, R.E. and Keoleian, G.A. (2008), "Design of green engineered cementitious composites for improved sustainability", *ACI Mater. J.*, **105**(6), 567-575.

Li, V.C. (1993), "From Micromechanics to Structural Engineering - the Design of Cementitous Composites for Civil Engineering Applications", *JSCE J. Struct. Mech. Earthq. Eng.*, **10**(2), 37-48. https://doi.org/10.2208/jscej.1993.471_1

Li, V.C. and Yang, E.-H. (2007), "Self Healing in Concrete Materials", In: van der Zwaag, S. (eds), Self Healing Materials, Springer Series in Materials Science, Vol. 100, Springer, Dordrecht, pp. 161-193. https://doi.org/10.1007/978-1-4020-6250-6_8

Liu, Z., Chen, X., Wang, X. and Diao, H. (2022), "Investigation on the dynamic compressive behavior of waste tires rubber-modified self-compacting concrete under multiple impacts loading", *J. Cleaner Product.*, **336**, 130289. https://doi.org/10.1016/j.jclepro.2021.130289

Mastali, M., Dalvand, A. and Sattarifard, A. (2017), "The impact resistance and mechanical properties of the reinforced self-compacting concrete incorporating recycled CFRP fiber with different lengths and dosages", *Compos. Part B: Eng.*, **112**, 74-92. https://doi.org/10.1016/j.compositesb.2016.12.029

Moghadam, A.S., Omidinasab, F. and Dalvand, A. (2020), "Experimental investigation of (FRSC) cementitious composite functionally graded slabs under projectile and drop weight impacts", *Constr. Build. Mater.*, **237**, 117522. https://doi.org/10.1016/j.conbuildmat.2019.117522

Muttashar, H.L., Ariffin, M.A.M., Hussein, M.N., Hussin, M.W. and Ishaq, S.B. (2018), "Self-compacting geopolymer concrete with spend garnet as sand replacement", *J. Build. Eng.*, **15**, 85-94. https://doi.org/10.1016/j.jobe.2017.10.007

Naaman, A.E. and Reinhardt, H.W. (2003), "High Performance Fiber Reinforced Cement Composites HPFRCC-4: International RILEM Workshop", *Mater. Struct.*, **36**, 710-712. https://doi.org/10.1007/BF02479507

Naghibdehi, M.G., Mastali, M., Sharbatdar, M.K. and Naghibdehi, M.G. (2014), "Flexural performance of functionally graded RC cross-section with steel and PP fibres", *Magaz. Concrete Res.*, **66**(5), 219-233. https://doi.org/10.1680/macr.13.00248

Okamura, H. and Ouchi, M. (1998), "Self-compacting high performance concrete", *Progress Struct. Eng. Mater.*, **1**(4), 378-383. https://doi.org/10.1002/pse.2260010406

Okamura, H. and Ozawa, K. (1994), "Self-compactable high-performance concrete in Japan", *Proceedings of the International Workshop on High-Performance Concrete*, ACI SP-159, (P. Zia, ed.), American Concrete Institute (ACI), Farmington Hills, MI, USA, pp. 31-44.

Oluokun, F.A., Burdette, E.G. and Deatherage, J.H. (1991), "Splitting tensile strength and compressive strength relationships at early ages", *ACI Mater. J.*, **88**(2), 115-121.

Ozawa, K., Maekawa, K. and Okamura, H. (1996), "Self-compacting high-performance concrete", Collected Papers (University of Tokyo: Department of Civil Engineering), **34**, 135-149.

Romualdi, J.P. and Mandel, J.A. (1964), "Tensile strength of concrete affected by uniformly distributed and closely spaced short lengths of wire reinforcement", *ACI* (*American Concrete Institute*) *Journal Proceedings*, **61**(6), 657-672. https://doi.org/10.14359/7801

Sahraoui, M. and Bouziani, T. (2019), "Effect of coarse aggregates and sand contents on workability and static stability of self-compacting concrete", *Adv. Concrete Constr., Int. J.*, **7**(2), 97-105. https://doi.org/10.12989/acc.2019.7.2.097

Salhi, M., Ghrici, M., Li, A. and Bilir, T. (2017), "Effect of curing treatments on the material properties of hardened self-compacting concrete", *Adv. Concrete Constr., Int. J.*, **5**(4), 359-375. https://doi.org/10.12989/acc.2017.5.4.359

Şengel, S., Erol, H., Yılmaz, T. and Anıl, Ö. (2022), "Investigation of the effects of impactor geometry on impact behavior of reinforced concrete slabs", *Eng. Struct.*, **263**, 114429. https://doi.org/10.1016/j.engstruct.2022.114429

Senthil, K., Satyanarayanan, K.S. and Rupali, S. (2016), "Energy absorption of fibrous self compacting reinforced concrete system", *Adv. Concrete Constr., Int. J.*, **4**(1), 37-47.

https://doi.org/10.12989/acc.2016.4.1.037
Valizadeh, A., Hamidi, F., Aslani, F. and Shaikh, F.U.A. (2020), "The effect of specimen geometry on the compressive and tensile strengths of self-compacting rubberised concrete containing waste rubber granules", *Structures*, **27**, 1646-1659. https://doi.org/10.1016/j.istruc.2020.07.069
Vandewalle, L., Nemegeer, D., Balazs, L., Barr, B., Barros, J., Bartos, P., Banthia, N., Criswell, M., Denarie, E., Di Prisco, M., Falkner, H., Gettu, R., Gopalaratnam, V., Groth, P., Häusler, V., Kooiman, A., Kovler, K., Massicotte, B., Mindess, S., Reinhardt, H.-W., Rossi, P., Schaerlaekens, S., Schumacher, P., Schnütgen, B., Shah, S., Skarendahl, A., Stang, H., Stroeven, P., Swamy, R., Tatnall, P., Teutsch, M. and Walraven, J. (2003), "Final recommendation of RILEM TC 162-TDF: Test and design methods for steel fibre reinforced concrete sigma-epsilon-design method", *Mater. Struct.*, **36**(262), 560-567. https://www.rilem.net/publication/publication/368?id_papier=7039
Vivek, S.S. and Dhinakaran, G. (2017), "Fresh and hardened properties of binary blend high strength self compacting concrete", *Eng. Sci. Technol.*, **20**(3), 1173-1179. https://doi.org/10.1016/j.jestch.2017.05.003
Wild, S., Sabir, B.B. and Khatib, J.M. (1995), "Factors influencing strength development of concrete containing silica fume", *Cement Concrete Res.*, **25**(7), 1567-1580. https://doi.org/10.1016/0008-8846(95)00150-B.
Xu, X., Ma, T. and Ning, J. (2019a), "Failure analytical model of reinforced concrete slab under impact loading", *Constr. Build. Mater.*, **223**, 679-691. https://doi.org/10.1016/j.conbuildmat.2019.07.008
Xu, X., Ma, T. and Ning, J. (2019b), "Failure mechanism of reinforced concrete subjected to projectile impact loading", *Eng. Fail. Anal.*, **96**, 468-483. https://doi.org/10.1016/j.engfailanal.2018.11.006
Zheng, J., Shen, F., Gu, X. and Zhang, Q. (2022), "Simulating failure behavior of reinforced concrete T-beam under impact loading by using peridynamics", *Int. J. Impact Eng.*, 165, 104231. https://doi.org/10.1016/j.ijimpeng.2022.104231
Zhu, W., Gibbs, J.C. and Bartos, P.J.M. (2001), "Uniformity of in situ properties of self-compacting concrete in full-scale structural elements", *Cement Concrete Compos.*, **23**(1), 57-64. https://doi.org/10.1016/S0958-9465(00)00053-6

CC